ARTICLE

Trapping of Metal Atoms in Vacancies of Carbon Nanotubes and Graphene

Julio A. Rodríguez-Manzo, Ovidiu Cretu, and Florian Banhart*

Institut de Physique et Chimie des Matériaux, UMR 7504 CNRS, Université de Strasbourg, 23 rue du Loess, 67034 Strasbourg, France

ABSTRACT Lattice defects in carbon nanotubes and graphene are created by focusing an electron beam in a scanning transmission electron microscope onto a 0.1 nm spot on the objects. Metal atoms migrating on the graphenic surfaces are observed to be trapped by these defects. Depending on the size of the defect, single metal atoms or clusters of several atoms can be localized in or on nanotubes or graphene layers. Subsequent escape of the metal atoms from the trapping centers gives information about the bonding between the metal atom and the defect. The process of trapping and detrapping is studied in a temperature range of 20—670 °C. The technique allows one to place metal atoms with almost atomic precision in graphenic structures and to create a predefined pattern of foreign atoms in graphene or carbon nanotubes.

KEYWORDS: carbon nanotubes · graphene · nanostructuring · *in situ* electron microscopy · lattice defects

Interactions between metals and graphitic carbon play an important role in different areas of nanotechnology.[1] One area is the synthesis of carbon nanotubes (CNTs) or graphene by chemical vapor deposition, which is based on the catalytic action of metals.[2−5] A detailed understanding of the interplay between catalytically active metals and the graphenic network before and during growth is mandatory for optimizing the synthesis. Another field of high importance is the interaction between metals and CNTs or graphene at metal−carbon interfaces in electrical contacts in devices or in composite materials for mechanical applications.[6−9] Due to the existence of covalent bonds between carbon and metal atoms, a large variety of composite nanostructures can be designed, but only very few possible systems (*e.g.*, CNT−metal junctions[10]) have been realized. Hence, this field promises an enormous potential in the development of new nanosystems with dedicated functions.

The design of such composite nanosystems from the bottom up would start with the replacement of single atoms, for example, a carbon atom in the lattice of a nanotube or a graphene layer by a metal atom. Such a procedure could be carried out by a chemical treatment, but without site selectivity. A more fundamental approach would be the generation of trapping centers in the graphenic network, that is, the generation of lattice vacancies that can trap metal atoms. Foreign atoms occupying vacancies in CNTs or graphene would be of particular interest in the context of doping.[11,12] The mechanisms of trapping and detrapping of dopant atoms as well as the mobility of substitutional atoms are subjects that have to be understood if the electrical properties of graphene-based materials are to be modified. If such a procedure can be carried out with atomic selectivity, the structuring of carbon-based systems in the presence of mobile metal atoms could be the basis of an atomic-scale design of new metal−carbon nanostructures. Here we address these issues by creating trapping centers in graphene and nanotubes with a highly focused electron beam and directly observing the trapping of individual metal atoms as well as metal clusters in defects.

RESULTS

Metal atoms (Fe, Co, and Mo) were deposited on samples of CNTs and graphene as described in the Methods section. Irradiation and imaging of the samples were carried out in the heating stage of a scanning transmission electron microscope (STEM). While scanning the beam over the specimen allowed imaging with almost 1 Å resolution, irradiation with a stationary beam was used to create defects at the atomic scale in a preselected position.[13] The beam was positioned by a dedicated program for the scan control.

*Address correspondence to banhart@ipcms.u-strasbg.fr.

Received for review February 22, 2010 and accepted May 19, 2010.

Published online May 25, 2010. 10.1021/nn100356q

© 2010 American Chemical Society

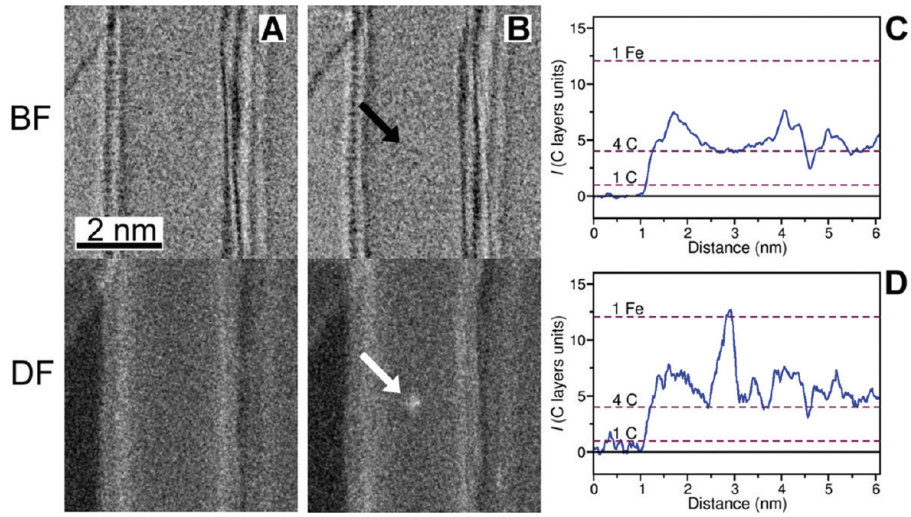

Figure 1. STEM images of a double-wall carbon nanotube before (A) and after (B) 10 s of spot irradiation at the position marked with the arrow. Bright-field (BF) and dark-field (DF) STEM images were taken simultaneously and are shown in the top and bottom row, respectively. (C,D) Intensity profiles along lines normal to the axis of the tube, taken from the DF image after irradiation (B). (C) Profile from an unmodified area next to the irradiated spot, averaged over 100 pixels in the direction of the tube; (D) profile through the spot, averaged over 8 pixels in the direction of the tube. The scattered intensity is normalized on the level of one layer of graphene, therefore giving 4 units at the center of the tube. The dashed lines represent the expected intensity levels for 1 or 4 layers of C and for 1 monolayer of Fe. Specimen temperature during the experiment = 475 °C.

After adjusting the desired temperature of the specimen, an area close to a metal particle lying on top of a CNT or a graphene flake was imaged by using both bright-field (BF) and dark-field (DF) detectors simultaneously. After recording an image from the initial state of the structure, the electron beam was directed onto a selected position of a nanotube or graphene layer for a few seconds in order to create a lattice defect. Then, several new scans were taken to monitor the behavior of the graphitic lattice and the metal atoms. In the BF mode, a coherent image of the structure is seen with moderate noise, whereas high-angle annular dark-field (HAADF) images give a directly interpretable incoherent image where the scattered intensity I depends on the atomic number Z of the element as $I \sim Z^{1.7}$.[14] Thus, metal atoms appear as bright dots in the DF images and can easily be distinguished from carbon-based materials.

Figure 1 shows the trapping of a metal atom at 475 °C in a region of a double-wall carbon nanotube (DWNT), where a defect has been produced by the focused electron beam. An image of the area of the sample that, besides DWNTs, contained Fe atoms and crystals was acquired prior to defect formation (Figure 1A). Afterward, the electron beam was directed onto a predefined position and kept stationary for 10 s ($\sim 10^5$ times the dwell time per pixel of the previous recording in the scanning mode). Immediately after spot irradiation, another image was recorded (Figure 1B), showing a bright spot in the dark-field image exactly at the site of previous spot irradiation. A quantitative analysis of the contrast in the DF image gives an increase of the scattered intensity in the irradiated spot of ~3.5 times relative to the center of the pristine DWNT. Line intensity profiles taken from the DF image from the unmodified and from the irradiated DWNT areas are shown in Figure 1C,D, respectively. Dashed lines indicate the expected levels of intensity from one or four planar layers of carbon and from a hypothetical monatomic layer of Fe. Considering the expected intensity proportional to $Z^{1.7}$, the measured intensity of the peak in Figure 1D corresponds to one Fe atom. Therefore, we can assume that an Fe atom was trapped in a defect on the top or bottom side of the DWNT. The contrast of the Fe atom hardly appears in the BF image (Figure 1B) because different atomic numbers do not differ much in contrast under coherent imaging conditions.

The interaction of metal atoms with defects in CNTs is not restricted to single atoms. Figure 2A shows a 7-wall MWNT at 470 °C covered with Co nanoparticles. Spot irradiation for a longer period (200 s) caused an aggregation of several Co atoms (Figure 2B) in a large defect in the MWNT. By measuring the diameter of the Co cluster and the difference in the intensity profiles before and after cluster formation, we could estimate an aggregate of approximately 15 Co atoms. The size of the cluster is large enough to allow imaging in the BF image (Figure 2B). However, another image, taken approximately 500 s after irradiation, does not show the Co cluster anymore in both BF and DF (Figure 2C). This latter effect, which was frequently observed in our experiments, can be attributed to the escape of metal atoms from defects.

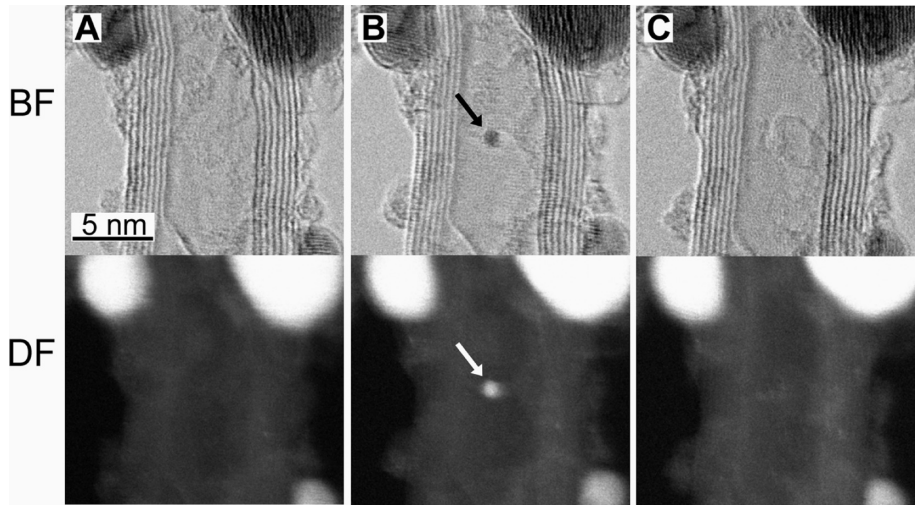

Figure 2. STEM images of a 7-wall MWNT at 475 °C. Simultaneously acquired BF and DF images are shown at the top and bottom, respectively. (A) MWNT prior to irradiation with some Co particles on the surface. (B) After spot irradiation for 200 s (one interval of 80 and another of 120 s interrupted by the acquisition of an image) at the area marked with an arrow. The dark spot in the BF image and the bright spot in the DF image indicate the trapping of Co atoms in the irradiated area of the MWNT. (C) Same area 500 s after spot irradiation. The contrast from the Co aggregate has vanished.

For single-wall carbon nanotubes (SWNTs), the effect of metal trapping was completely absent in the whole investigated temperature range of 20−500 °C. For DWNTs or MWNTs, the trapping effect was only observable at temperatures of 240 °C and above. The effect did not occur at room temperature. These observations also prove that in our experiments the obtained intensity profiles from DF STEM images are not caused by hydrocarbon contamination.

The effect of metal trapping was also observed in graphene. Sheets consisting of 1−20 graphene layers with Ni or Mo crystals on the surface were irradiated and imaged at different temperatures under the same conditions as CNTs. Figure 3 shows the effects of irradiation on the same area of a sample covered with Mo crystals at two different temperatures. Intensity profiles taken from the graphene flake in lower-magnification DF images of the same area indicate a thickness of approximately 6 graphene monolayers. At 300 °C (Figure 3A,B), 30 s of spot irradiation creates a larger defect complex (visible as a hole in both BF and DF images) in the graphenic lattice, which is completely refilled by carbon atoms about 1 min after irradiation (the hole does not appear anymore). However, at 400 °C (Figure 3C,D), the same experiment produces a defect that is instantly filled with a cluster of Mo atoms.

In another experiment (Figure 4), repeated scans of a thicker multilayer graphene area (~16 layers estimated from DF image profiles) were taken until the uniformly irradiated area was covered with scattered individual Mo atoms that stem from the metal crystals nearby. This can be seen in Figure 4A by the large number of spots in both BF and DF images. Then we programmed the scan to carry out irradiations on a number of spots (30 s at each spot) in a predefined triangular pattern. This led to the trapping of Mo atoms in the pattern of defects, as

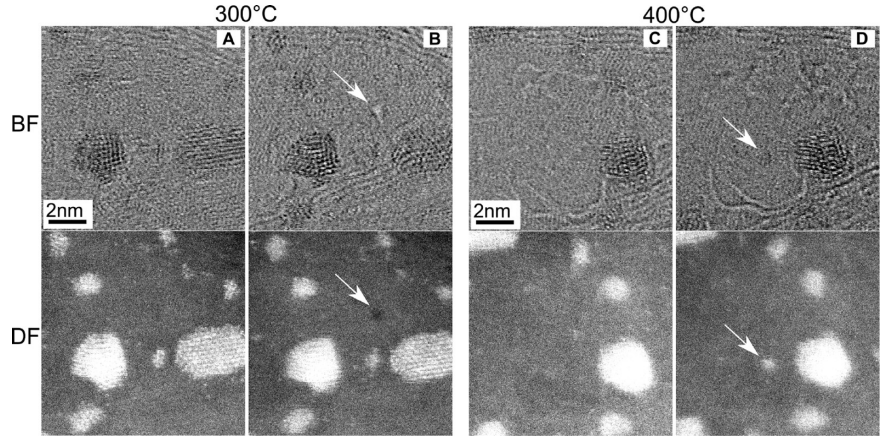

Figure 3. Trapping of Mo atoms at defects in graphene. At 300 °C (A,B), a hole is created in the graphene layer by concentrating the electron beam for 30 s onto the area marked with an arrow. No trapping of Mo atoms occurs. At 400 °C (C,D), the same experiment in the same area leads to the trapping of Mo atoms (arrowed).

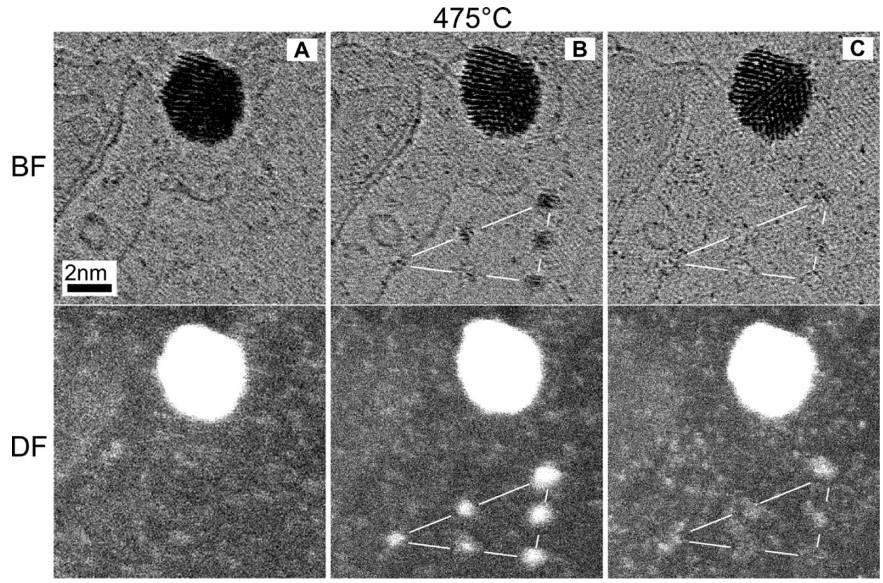

Figure 4. Patterning of a graphene sheet by an automatic electron beam control. Mo atoms are trapped by the large vacancies created by focusing the electron beam on a triangular set of spots (indicated by lines) for 30 s in each spot. Before irradiation (A), immediately after irradiation (B), and 40 min after irradiation (C). Temperature = 475 °C.

shown in Figure 4B. As in the case of CNTs, detrapping of the Mo atoms from the graphene sheet was observed, as well. This is visible in Figure 4C, which was taken 40 min after the experiment (no electron irradiation was carried out between B and C); there are significantly less trapped atoms than in the previous images, but a certain number of Mo atoms remain trapped in the irradiated area.

Figure 5 shows the creation of a larger hole in a double-layer graphene sheet. DF intensity profiles indicate that only one layer has been removed in the hole. Figure 5A shows the area before creation of the hole. A Moiré pattern corresponding to two graphene layers rotated by about 30° relative to each other appears. The area inside the dotted rectangle is shown before (Figure 5B) and immediately after 4 s of spot irradiation (Figure 5C) as DF images. The inset of Figure 5C is a 3D representation of the intensity in the highlighted area. Judging by the peaks at the edge of the hole, a few single Mo atoms on the surface were trapped at the border of this large vacancy; some of them were later seen to escape (the sample temperature was 670 °C in this experiment).

DISCUSSION

Different types of interactions between metal atoms and graphenic lattices can be distinguished. Metal atoms can either be located on top of a coherent (nondefective) graphenic plane in a weakly bonded adatom configuration or form covalent bonds with carbon atoms at the edge of a graphenic layer or at defective sites such as a lattice vacancy or a reconstructed area.[15,16] The behavior of metal atoms in these configurations is completely different. While adatoms on a perfect surface are highly mobile, metal atoms occupying defective sites in CNTs or graphene can be trapped in more or less stable positions.[17] The migration of metal atoms on top of or within graphenic lattices has already been studied both experimentally[18] and theoretically.[17,19]

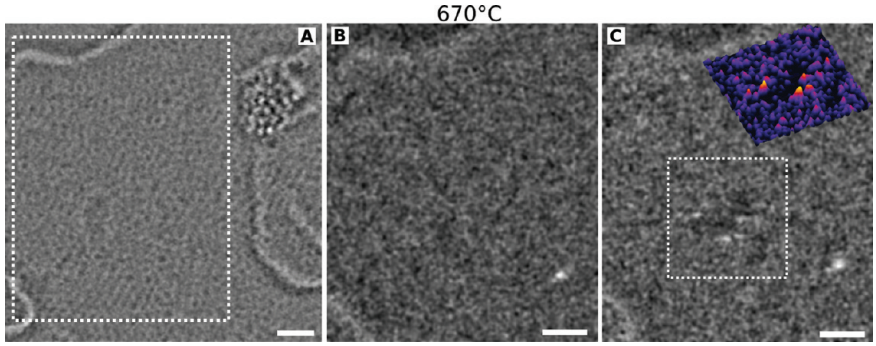

Figure 5. Trapping of a few Mo atoms in a double-layer graphene sheet. A hole of approximately 1 nm in diameter was made by irradiating an area inside the rectangle in (A) for 4 s. The area is shown before (B) and after (C) irradiation. The inset in (C) is a 3D intensity profile of the area inside the rectangle. Some Mo atoms trapped at the edge of the hole are visible as bright dots in (C). Scale bars are 1 nm. All three images have been processed with a band-pass filter. Specimen temperature = 670 °C.

While adatoms diffuse fast and have low activation energies, diffusion in the lattice *via* substitutional sites occurs at a much slower rate because the breaking of covalent bonds in the host lattice requires higher activation energies.

We first have to consider the generation of vacancies by the ballistic ejection of carbon atoms,[20] which is possible if the energy of the electrons is above the displacement threshold for graphitic structures. A threshold electron energy in the range of 80−100 keV for nanotubes and graphene has been reported.[21,22] In the present experiment, an electron energy of 200 keV was used. At a beam current density of $\sim 5 \times 10^5$ A cm^{-2}, a displacement rate of approximately 60 displacements per second can be expected for each carbon atom (if stationary carbon atoms are assumed).[13,23] Therefore, vacancies in nanotubes or graphene are created immediately under such an intense beam, as has already been demonstrated previously by the imaging of unfilled vacancies.[13] Under continuous scanning, as it is done for imaging a selected area, some vacancies are created randomly, whereas the stationary beam creates vacancies in the preselected position.

Vacancies act as trapping centers for carbon or metal atoms, thus leading to chemisorption with the formation of covalent bonds. The filling of vacancies depends on the availability of both species. A large number of highly mobile carbon atoms would anneal the defect immediately and hinder the trapping of metal atoms. Therefore, the concentration of metal atoms and their mobility must be high enough to allow the filling of vacancies. Metal atoms are detached from the small crystals on the nanotube or graphene surfaces. This process can be induced by electron irradiation as it was observed in this experiment under the scanning beam. The liberated metal adatoms diffuse on a graphitic surface with a diffusivity proportional to $\exp(-E_a/kT)$ where E_a is the activation energy for migration. Theoretical studies for metal adatom adsorption and diffusion on perfect graphene revealed activation energies in the range of 0.14−0.8 eV.[17,24,25] These values have been confirmed by experimental measurements, for example, 0.28 eV for Au on graphite.[26] The low activation energies ensure a high mobility of the metal atoms on a perfect graphitic layer even at room temperature (with $E_a = 0.2$ eV, an atom migrates over a mean distance of 10 μm in 1 s at room temperature). Hence, an adsorption of atoms on perfect graphene can be excluded, and surface diffusion is much too fast to allow monitoring of the atoms in the STEM where an image scan needs typically several seconds. On the other hand, surface diffusion is fast enough to lead to a wide distribution of migrating metal atoms on CNTs or graphene so that there is a high probability that the metal atoms are trapped in beam-induced vacancies.

The migration of a metal atom which is already trapped in a single or multiple vacancy would require the breaking of metal−carbon as well as carbon−carbon bonds and has therefore a much higher activation energy than surface diffusion. An earlier experimental study revealed activation energies of 2.5 eV for the in-plane migration of both Au and Pt atoms in graphene and 2.3 eV for the migration of Pt atoms in the shells of multiwall CNTs.[18] Calculations are in rough agreement with the experimental data and predicted activation energies for diffusion in graphene in the range 2.1−3.6 eV for metal−monovacancy and around 5 eV for metal−divacancy complexes.[17] An intermediate scenario is the trapping of metal atoms on reconstructed areas of tubes or graphene where hexagonal rings have been replaced by pentagonal, heptagonal, or larger rings (no dangling bonds). Here, we expect a larger bonding energy than for an atom on a perfect graphenic lattice due to the increased reactivity of such nonhexagonal defects (the metal d-orbitals bind to the distorted graphitic π-electron system). Finally, metal atoms can be trapped at the edge of a larger vacancy complex where dangling bonds are available.

In the present experiment, the vacancies created by the beam are, in many cases, certainly larger than single vacancies. This is due to the irradiation times of several seconds and a slight drift of the specimen during irradiation. We observe that the vacancy−metal complexes are stationary for a certain time. However, the escape of metal atoms from the vacancies occurred in many cases. Therefore, the bonding between metal and carbon is, at least in some defect configurations, not strong enough to withstand thermal excitation. Detrapping *via* electron irradiation[27] has to be taken into account, as well. However, the irradiation of a trapped metal atom occurs for only $\sim 10^{-3}$ s during an image scan, and the displacement of metal atoms requires large momentum transfers (the displacement rate is smaller than for carbon atoms). Furthermore, the period between two scans was very long (*e.g.*, 500 s in the example in Figure 2); therefore, beam-induced detrapping seems less likely in this case, at least at higher temperatures.

The binding energies of metal atoms in vacancies in graphene are quite high, typically 7 eV for an Fe atom in a single vacancy and 6 eV for Fe in a double vacancy.[17] Such high energies would not allow detrapping under our experimental conditions, neither thermally nor by irradiation. If a metal atom is sitting at the edge of a graphene layer, only one or two bonds per metal atom can be formed, and bonding with an energy of approximately 3−4 eV can be

assumed (roughly half of the binding energy in a vacancy). Nevertheless, such a binding energy would still be too high for allowing thermal detrapping of metal atoms at moderate temperatures. The detrapping of single metal atoms from defects that we observe points to a lower binding energy of the atom to the defect. A reconstructed area (combination of five- and seven-membered rings) could serve as such a trapping center. The detrapping of larger metal clusters (Figures 2 and 4) can be explained in terms of a lower inherent stability of the cluster. A decay of the cluster with a dispersion of the metal atoms and a refilling of the defect with carbon atoms could be energetically favorable. Nevertheless, as seen in Figure 4, some atoms remain trapped in larger defects, so we have to assume that these atoms form strong bonds to carbon atoms at the edges.

The fact that trapping of metal atoms in SWNTs was not observed can be related to the instability of vacancies in SWNTs due to a rapid reconstruction of the lattice.[13,28] However, nonhexagonal rings should exist in SWNTs after the reconstruction and act as weak trapping sites. To answer the question why trapping does not happen in SWNTs, a computational study, taking the high curvature of the graphitic layers into account, would have to be undertaken.

To summarize the scenarios, it appears that the trapping of *single* metal atoms (Figure 1) occurs on a reconstructed area of a graphenic system with more than one layer. Intershell bonds between carbon atoms may exist and stabilize these defects against annealing.[13] Even if no dangling bonds exist at such defects, the strongly distorted π-electron system may form bonds of sufficient strength to the metal atoms. If larger defects (multiple vacancies) are generated, bonding to single metal atoms (Figure 5) can occur readily at the edges of the hole where dangling bonds are available. However, the observation of detrapping shows that strong covalent bonding to a single metal atom in a vacancy does not exist. The trapping of larger metal clusters (Figures 2 and 4) can be explained by a covalent bonding of some metal atoms at the edges of larger defects, followed by the aggregation (crystallization) of further metal atoms that finally leads to a filling of the hole.

CONCLUSIONS

The present experiments show that it is possible to create atomic-scale defects in MWNTs and in graphene in preselected positions with a focused electron beam and to use these defects as trapping centers for foreign atoms. By applying such a technique of subnanometer structuring, metal atoms can be placed in selected locations in graphene or nanotubes. The method can make use of computer-assisted patterning as applied in electron beam lithography but can be carried out on an atomic scale. The deleterious effect of detrapping that we have observed in some cases could be suppressed by cooling the sample after the trapping and avoiding further irradiation. The decoration of graphene layers or carbon nanotubes with metal atoms in predefined locations could be of interest in the modification of the electronic or magnetic properties of these species. A system of quantum dots[29] can be made in such a way, leading to stationary electron waves in these patterned graphenic sheets and enabling us to design devices with new functions.

METHODS

Samples containing CNTs and metals were made in two different ways. Commercial samples (Thomas Swan & Co. Ltd.) of single- and double-wall carbon nanotubes containing residues of the Fe catalyst were used for studying the interaction of Fe atoms with CNTs. The interaction with Co was studied by synthesizing multiwall carbon nanotubes by CVD,[30] which were then covered with a 5 nm layer of Co in a sputtering chamber.[31] The CNT samples were placed on standard Cu grids for investigation in a transmission electron microscope (TEM).

Layers of graphene were obtained by mechanical exfoliation from HOPG (highly oriented pyrolytic graphite) crystals ("Scotch tape method").[5] The graphene flakes were dispersed in acetone, and a drop of the dispersion was placed on a standard TEM grid (Ni or Mo) and dried. The grids with graphene flakes were annealed at high temperatures (1000−2000 °C, depending on the type of the grid) in a graphite or tungsten crucible in a vacuum furnace (10^{-7} mbar) that was heated by an electron beam. Besides improving the quality of the graphene flakes,[32] the annealing provides metal atoms that evaporate from the TEM grid onto the graphene layers, where most of them agglomerate into nanometer-sized metal crystals.

An electron microscope (JEOL 2100F), equipped with an aberration corrector for the condenser and operated in the scanning transmission electron microscopy (STEM) mode at 200 kV, was used for both imaging and electron irradiation. The specimens were mounted in a dedicated heating stage, which allows heating up to 800 °C inside the microscope column (10^{-7} mbar). The electron beam had a diameter of 1.1 Å and a current density of 5×10^5 A cm^{-2} on the specimen. The beam convergence semiangle was 25 mrad, and the detection semiangle in DF images was 35−90 mrad. To avoid hydrocarbon contamination (which is often a severe problem in STEM), the specimens were heated inside the TEM column at temperatures above 400 °C prior to all experiments.

Acknowledgment. Funding by the Région Alsace (480-09), the Agence Nationale de Recherche (ANR-09-BLAN-0363-01), and by the Ministère de l'Enseignement Supérieur et de la Recherche is gratefully acknowledged.

REFERENCES AND NOTES

1. Banhart, F. Interactions between Metals and Carbon Nanotubes: At the Interface between Old and New Materials. *Nanoscale* **2009**, *1*, 201–213.
2. Vajtai, R.; Wei, Q. W.; Ajayan, P. M. Controlled Growth of Carbon Nanotubes. *Philos. Trans. R. Soc. London, Ser. A* **2004**, *362*, 2143–2160.

3. *Understanding Carbon Nanotubes* (Lecture Notes in Physics 677); Loiseau, A., Launois, P., Petit, P., Roche, S., Salvetat, J. P., Eds.; Springer: Berlin and Heidelberg, 2006.
4. Harris, P. J. F. *Carbon Nanotube Science*; Cambridge University Press: New York, 2009.
5. Geim, A. K. Graphene: Status and Prospects. *Science* **2009**, *324*, 1530–1534.
6. Avouris, P. Molecular Electronics with Carbon Nanotubes. *Acc. Chem. Res.* **2002**, *35*, 1026–1034.
7. Anantram, M. P.; Léonard, F. Physics of Carbon Nanotube Electronic Devices. *Rep. Prog. Phys.* **2006**, *69*, 507–561.
8. Charlier, J.-C.; Blase, X.; Roche, S. Electronic and Transport Properties of Nanotubes. *Rev. Mod. Phys.* **2007**, *79*, 677–732.
9. Lu, W.; Lieber, C. M. Nanoelectronics from the Bottom Up. *Nat. Mater.* **2007**, *6*, 841–850.
10. Rodríguez-Manzo, J. A.; Banhart, F.; Terrones, M.; Terrones, H.; Grobert, N.; Ajayan, P. M.; Sumpter, B. G.; Meunier, V.; Wang, M.; Bando, Y.; Golberg, D. Heterojunctions between Metals and Carbon Nanotubes as Ultimate Nanocontacts. *Proc. Natl. Acad. Sci. U.S.A.* **2009**, *106*, 4591–4595.
11. Zhou, C.; Kong, J.; Yenilmez, E.; Dai, H. Modulated Chemical Doping of Individual Carbon Nanotubes. *Science* **2000**, *290*, 1552–1555.
12. Maciel, I. O.; Anderson, N.; Pimenta, M. A.; Hartschuh, A.; Qian, H.; Terrones, M.; Terrones, H.; Campos-Delgado, J.; Rao, A. M.; Novotny, L.; Jorio, A. Electron and Phonon Renormalization near Charged Defects in Carbon Nanotubes. *Nat. Mater.* **2008**, *7*, 878–883.
13. Rodriguez-Manzo, J. A.; Banhart, F. Creation of Individual Vacancies in Carbon Nanotubes by Using an Electron Beam of 1 Å Diameter. *Nano Lett.* **2009**, *9*, 2285–2289.
14. Voyles, P. M.; Grazul, J. L.; Muller, D. A. Imaging Individual Atoms Inside Crystals with ADF-STEM. *Ultramicroscopy* **2003**, *96*, 251–273.
15. Palacios, J. J.; Pérez-Jiménez, A. J.; Louis, E.; SanFabián, E.; Vergés, J. A. First-Principles Phase-Coherent Transport in Metallic Nanotubes with Realistic Contacts. *Phys. Rev. Lett.* **2003**, *90*, 106801.
16. Nemec, N.; Tománek, D.; Cuniberti, G. Contact Dependence of Carrier Injection in Carbon Nanotubes: An *Ab Initio* Study. *Phys. Rev. Lett.* **2006**, *96*, 076802.
17. Krasheninnikov, A. V.; Lehtinen, P. O.; Foster, A. S.; Pyykkö, P.; Nieminen, R. M. Embedding Transition Metal Atoms in Graphene: Structure, Bonding, and Magnetism. *Phys. Rev. Lett.* **2009**, *102*, 126807.
18. Gan, Y.; Sun, L.; Banhart, F. One- and Two-Dimensional Diffusion of Metal Atoms in Graphene. *Small* **2008**, *4*, 587–591.
19. Zhuang, H. L.; Zheng, G. P.; Soh, A. K. Interactions between Transition Metals and Defective Carbon Nanotubes. *Comput. Mater. Sci.* **2008**, *43*, 823–828.
20. Krasheninnikov, A. V.; Banhart, F. Engineering of Nanostructured Carbon Materials with Electron or Ion Beams. *Nat. Mater.* **2007**, *6*, 723–733.
21. Smith, B. W.; Luzzi, D. E. Electron Irradiation Effects in Single Wall Carbon Nanotubes. *J. Appl. Phys.* **2001**, *90*, 3509–3515.
22. Zobelli, A.; Gloter, A.; Ewels, C. P.; Seifert, G.; Colliex, C. Electron Knock-on Cross Section of Carbon and Boron Nitride Nanotubes. *Phys. Rev. B* **2007**, *75*, 245402.
23. Banhart, F. Irradiation Effects in Carbon Nanostructures. *Rep. Prog. Phys.* **1999**, *62*, 1181–1221.
24. Kong, K.; Choi, Y.; Ryu, B.; Lee, J.; Chang, H. Investigation of Metal/Carbon-Related Materials for Fuel Cell Applications by Electronic Structure Calculations. *Mater. Sci. Eng., C* **2006**, *26*, 1207–1210.
25. Chan, K. T.; Neaton, J. B.; Cohen, M. L. First-Principles Study of Metal Adatom Adsorption on Graphene. *Phys. Rev. B* **2008**, *77*, 235430.
26. Anton, R.; Schneidereit, I. *In Situ* TEM Investigations of Dendritic Growth of Au Particles on HOPG. *Phys. Rev. B* **1998**, *58*, 13874–13881.
27. Malola, S.; Häkkinen, H.; Koskinen, P. Gold in Graphene: In-Plane Adsorption and Diffusion. *Appl. Phys. Lett.* **2009**, *94*, 043106.
28. Kotakoski, J.; Krasheninnikov, A. V.; Nordlund, K. Energetics, Structure, and Long-Range Interaction of Vacancy-Type Defects in Carbon Nanotubes: Atomistic Simulations. *Phys. Rev. B* **2006**, *74*, 245420.
29. Pedersen, T. G.; Flindt, C.; Pedersen, J.; Mortensen, N. A.; Jauho, A.-P.; Pedersen, K. Graphene Antidot Lattices: Designed Defects and Spin Qubits. *Phys. Rev. Lett.* **2008**, *100*, 136804.
30. Janowska, I.; Winé, G.; Ledoux, M.; Pham-Huu, C. Structured Silica Reactor with Aligned Carbon Nanotubes as Catalyst Support for Liquid-Phase Reaction. *J. Mol. Catal. A* **2007**, *267*, 92–97.
31. Zhang, Y.; Dai, H. Formation of Metal Nanowires on Suspended Single-Walled Carbon Nanotubes. *Appl. Phys. Lett.* **2000**, *77*, 3015–3017.
32. Liu, Z.; Suenaga, K.; Harris, P. J. F.; Iijima, S. Open and Closed Edges of Graphene Layers. *Phys. Rev. Lett.* **2009**, *102*, 015501.